This is a repository copy of *Localized and General Corrosion Characteristics of Carbon Steel in H2S Environments*.

White Rose Research Online URL for this paper:
http://eprints.whiterose.ac.uk/144402/

Version: Accepted Version

Localized and general corrosion characteristics of carbon steel in H$_2$S environments

Frederick Pessu[1], Yong Hua[1], Wassim Taleb[1] Thibaut Chapentier[1], Richard Barker[1] Fakuen Chang[2], Tao Chen[2], and Anne Neville[1]

[1]Institute of Functional Surfaces, Faculty of Mechanical Engineering, University of Leeds, Leeds, United Kingdom, LS2 9JT

[2]Exploration and Petroleum Engineering Advanced Research Centre (EXPEC ARC) Saudi Aramco

ABSTRACT

Carbon steel remains the most commonly used material in oilfield applications. The susceptibility of carbon steel to various forms of corrosion is one of the major drawbacks to its economic and metallurgical advantages. The formation of Iron Sulfide (FeS) corrosion product is common during its application in H$_2$S-containing environments. The plurality of mechanisms is a fundamental aspect of FeS formation that is still not clearly understood especially in H$_2$S/CO$_2$ environments. Localized and/or pitting corrosion of carbon steel occurring in oilfields is also an aspect of the corrosion process that is of increasing concern and linked to these environments. Pitting corrosion is known to be the most unpredictable form of corrosion and, as such, it is difficult to mitigate against. The nature of the environment is seen as a key contributor to the evolution of FeS corrosion product and the occurrence of localized and/or pitting corrosion, especially in complex oilfield environments containing H$_2$S, CO$_2$ and other acid gases. In addition, multiple cations such as Fe^{2+}, Ca^{2+} and Mg^{2+} can further complicate the system. The presence of such cations in the brine chemistry could also impact the properties and chemistry of FeS films and the localized and/or pitting corrosion behavior of exposed carbon steel materials. This work focuses on understanding FeS formation kinetics and corrosion damage characteristics in different 10% H$_2$S-containing environments in 1M NaCl brine and Forties brine containing Ca^{2+}, Mg^{2+}, Ba^{2+} and Sr^{2+}. Linear polarization resistance (LPR) measurements combined with post-experiment surface analysis such as XRD and SEM are used to understand aspects of the localized and general corrosion behavior. The brine solutions are saturated with different sour corrosion systems; 10% H$_2$S - 90%CO$_2$ at 80°C. The relationship between the processes of FeS formation and evolution of localized and/pitting corrosion is established.

Key words: H$_2$S, CO$_2$, FeS, uniform corrosion, pitting corrosion, Ca^{2+}, Mg^{2+}, Fe^{2+}.

INTRODUCTION

The evaluation of carbon steel used in oil and gas corrosion environments is important to help minimize the costly economic and human losses due to corrosion [1, 2]. Corrosion in oilfield environments is mainly

associated with the presence of dissolved acidic gases in reservoir brines such as CO_2 and/or H_2S[2]. The presence of H_2S has been reported to introduce some complexities to the corrosion mechanism[3, 4] and previous studies have also reported the H_2S corrosion process to consist of both direct reduction of H_2S at the surface and an aqueous phase reaction[5-7]. It has been shown that these different electrochemical pathways lead to different types and morphologies of FeS such as mackinawite, cubic ferrous sulfide, pyrrhotite, troilite, pyrite, or greigite[8, 9]. However, the most common type of FeS is mackinawite and the formation of other forms is dependent on process parameters such as temperature, H_2S concentration in ratio combination with either CO_2 or other more inert gases and immersion time [4, 10].

The ability of FeS formed to protect against uniform corrosion has also been established over a wide range of operating conditions [8, 10, 11]. Protectiveness of FeS was also shown in a recent publication[10] as being achievable over 7 days test duration with the formation of different crystal structures and FeS morphologies. One key distinctive consequence of changes in concentration of H_2S gas and hence nature of FeS formed was in the severity and morphology of pitting corrosion attack. It was established that a combination of high H_2S content and presence of CO_2 helps to promote severe pitting at 80°C after 7 days [9, 10]. The role of CO_2 in H_2S-dominated corrosion environments relates to the role of CO_2 in accelerating metal dissolution and promoting more FeS formation via precipitation.

In the scenario of a typical oilfield environment, the formation/injection water may contain a wide range of cations such as Ca^{2+}, Mg^{2+}, Ba^{2+} and K^+ and Fe^{2+}. Fe^{2+} may be flowing down from other areas of the system already experiencing corrosion. The effect of such cationic variance on the corrosion characteristics (pitting and general corrosion) has not been given sufficient research attention. In the context of a CO_2 environment, it was recently shown by Hua et al[12] at 100 bar partial pressure of CO_2 and 60°C that Ca^{2+} can interact with $FeCO_3$ in CO_2 environment, resulting in the formation of iron-calcium carbonate ($Fe_xCa_{1-x}CO_3$). The molar fractions of Fe and Ca within the product vary with Ca^{2+} concentration in the solution. This was also found to impact the corrosion characteristics on carbon steel exposed to this environment. Both Hua et al.[12] and Jiang et al[13] reported that there was a reduction in corrosion rate with the presence of Ca^{2+} in the brine, which influenced the chemistry and composition of the corrosion product. However, Hua et al[12] also reported an increase in the severity of pitting corrosion with increasing Ca^{2+} concentration.

The presence of cations such as additional (Fe^{2+}, Ca^{2+} and Mg^{2+}) could be influential in H_2S-containing environments and the corrosion interface. However, limited research has been carried out in the area of sour corrosion of carbon steel with complex brine chemistries. It is believed that the increased propensity of FeS to reduce uniform corrosion and promote pitting corrosion initiation already established in a previous publication[9], can be affected by the presence of additional concentration of Fe^{2+}, Ca^{2+}, Mg^{2+}, Ba^{2+} and Sr^{2+}. Therefore, this study aims to identify the role of Ca^{2+} and Mg^{2+} ions on the formation, morphology and chemistry of FeS corrosion products developed in H_2S-containing environments. In addition, the work seeks to determine the relationship between the corrosion products, solution chemistry and the extent of uniform and pitting corrosion of carbon steel in different H_2S-containing brines.

EXPERIMENTAL PROCEDURE

The experiments were conducted in a 1M NaCl and Forties brine containing ~3000 ppm of Ca^{2+}, ~1200 ppm of Mg^{2+}, ~52 ppm Ba^{2+} and ~150 ppm Sr^{2+} at 80°C with emphasis on investigating corrosion product formation and morphology, quantification of uniform corrosion rates and the extent and morphology of pitting corrosion. A pre-mixed gas phase composition of 10% H_2S and 90% CO_2 was used as the gas phase composition above the test solution in this study. It is important to note here that the pH of the test systems was not controlled and monitored but allowed to evolve as the corrosion processes occurred.

2

<u>Materials:</u> X65 carbon steel (UNS K03014) samples were used as the working electrodes within a three-electrode cell in each experiment. The steel possessed a ferritic/pearlitic microstructure. The nominal composition of X65 (UNS K03014) steel is provided in Table 1.

Table 1: Elemental composition of X65 (UNS K03014) steel (wt. %)

C	Si	P	S	Mo	Mn	Ni	Nb	V	Fe
0.15	0.22	0.023	0.002	0.17	1.42	0.09	0.05	0.06	97.81

The carbon steel was sectioned into 10 mm x 10 mm x 5 mm samples. Wires were soldered to the back of each test specimen and then embedded in a non-conducting resin. Prior to the start of each experiment, test samples were wet-ground with 1200 silicon carbide grit paper, degreased with acetone, rinsed with distilled water and dried with compressed air before immersion into the test brine. A surface area of 1 cm^2 was exposed to the electrolyte per sample and 5 samples were used per liter of solution.

<u>Brine chemistry and experiment matrix</u>: Three different brine chemistries were used in this study. They are designated as Brine 1 and Brine 2 as shown in Table 2.

Table 2: Brine chemistry

Test Solution	Brine Chemistry	
Brine 1 (Simple brine)	1M NaCl	
Brine 2	1M NaCl + 50 ppm of Fe^{2+}	
Brine 3 (Forties Brine)	NaCl	42.97g/L
	KCl	0.18g/L
	$CaCl_2.2H_2O$	11.00g/L
	$MgCl_2.6H_2O$	10.17g/L
	$BaCl_2.2H_2O$	0.09g/L
	$SrCl_2.6H_2O$	0.46g/L

<u>Experimental setup:</u> Sour (H_2S) corrosion experiments are conducted in a 1 liter autoclave as shown in Figure 1. The test solution was deaerated for a minimum of 12 hours using N_2 in a 316 SS (UNS S31600) vessel before it is carefully pumped into an already deaerated test vessel (Hastelloy-UNSN10276) containing 5 samples safely embedded in resin and suspended within it with wires attached to each for electrochemical measurements. The test solution inside the autoclave was not stirred during these tests. The corrosion potential is used to monitor the moment at which H_2S gas being introduced into the test vessel comes in contact with the samples already immersed in a N_2 saturated solution. The corrosion potential was ~ -730 mV/decade for N_2 saturated systems and increased to~ -680 mV/decade once the fed H_2S gas was introduced into the test environment inside the Hastelloy (UNSN10276) test vessel for the first time. Prior to the transfer of electrolyte into the test vessel, the temperature of the electrolyte was heated to 80˚C in the 316 SS (UNS S31600) vessel. Heat loss during the transfer of test solution was regained by heating the test vessel (usually at 60-65˚C) back to 80˚C before the introduction of H_2S/CO_2 gas mixtures. The tests were conducted in the autoclave at ambient pressure and safely sealed. Electrochemistry was started once the H_2S gas supply was turned on. The exit line of the test vessel was channeled into a 2L 316 SS autoclave with a PTFE liner containing 10 wt. % NaOH and 3 other polymer vessels containing Jasorb G-15 scrubbing pellets.

At the end of the experiments, samples are removed for SEM imaging/EDX and XRD analysis. Other samples were chemically cleaned to remove all traces of corrosion products before using profilometry to determine the extent of pitting corrosion on the steel surface. The cleaning process consisted of wiping the surface with a cotton pad soaked in Clarke's solution (20 g antimony trioxide + 50 g stannous chloride + 1000 ml 38% hydrochloric acid) in accordance with ASTM Standard G1-03,

washed, air dried, and carefully stored in a de-aerated chamber to avoid oxidation prior to surface analysis. Pitting corrosion analysis was carried out using the NPFLEX 3D[1] interferometer.

<u>Addition of 50 ppm of Fe^{2+}:</u> 50 ppm (~0.11g of $FeCl_2$ per 1000 ml of brine) is added into N_2 saturated solution before it is pumped into the already sealed autoclave test vessel.
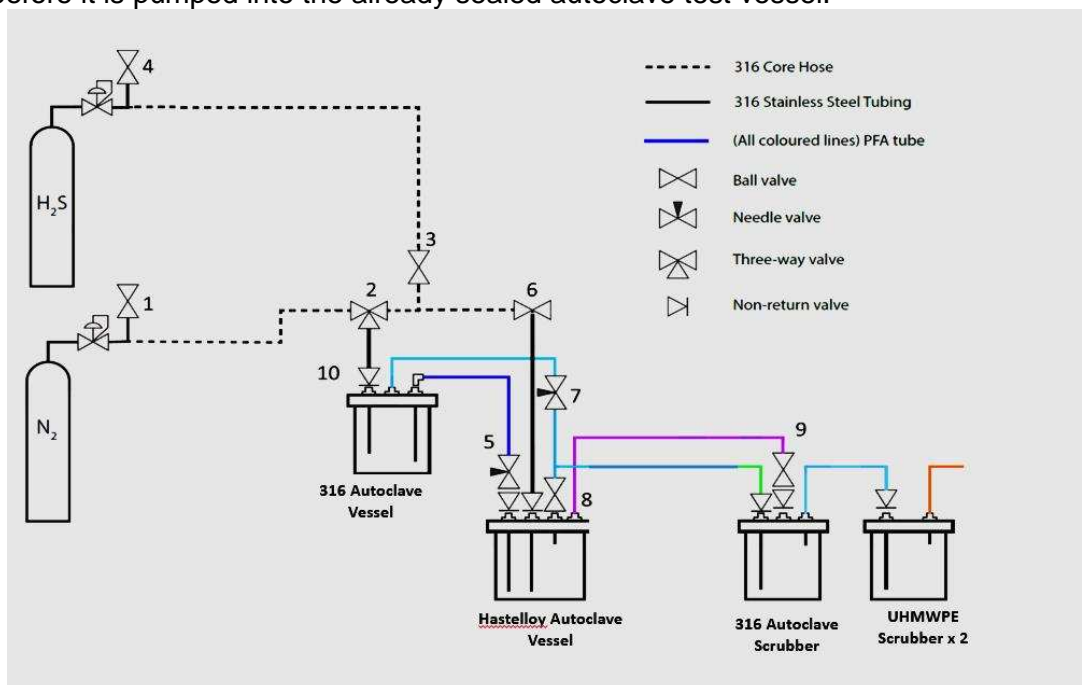
Figure 1 schematic representation of the experimental system layout.

<u>In-situ electrochemical measurements:</u> Electrochemical measurements were conducted on one sample per test. Each sample formed the working electrode in a three-electrode cell which also comprised of an Ag/AgCl reference electrode and a platinum counter electrode. The tests were repeated between 3 to 5 times to ensure repeatability. All electrochemical measurements were conducted with an Ivium CompactStat[2] potentiostat. Linear Polarization Resistance (LPR) measurements were performed by polarizing the working electrode every 15 minutes from 15 mV below the Open Circuit Potential (OCP) to 15 mV more positive than OCP at a scan rate of 0.25 mV/s to determine the polarization resistance (R_p). Tafel constants (β_a and β_c) of 120 mV/decade were used in conjunction with R_p and Faraday's Law to determine the in-situ corrosion rates as a function of time for the experimental conditions under investigation in this study.

<u>Corrosion product identification:</u> XRD patterns were collected using a Bruker D8[3] equipped with a LynxEye[4] detector and a 90 position auto sampler, employing Cu Kα radiation with an active area of 1cm[2] programmable di-vergence slits. Scans were performed over a range 2Θ = 10 to 70° using a step size of 0.033 per second, with a total scan time of approximately 50 minutes. The results were analyzed using X'Pert[5] HighScore software and compared with individual crystal standards from the database.

<u>Characterization of pitting corrosion damage:</u> Surface profilometry was used in this study to evaluate pitting attack. Pit depth measurements were conducted in alignment with ASTM G46-94[6][14]. A 3D interferometer was used for obtaining the discrete geometry of pits on over 81% of the steel surface

---

[1] Trade name

[2] Trade name

[3] Trade name

[4] Trade name

[5] Trade name

[6] Trade name

(the remaining 19% represents the edges of the sample). Pits were identified based on carefully chosen thresholds. Thresholds were chosen with reference to the surface roughness of uniformly corroded areas. This enabled pits with distinct pit depths, diameters, and areas to be identified and quantified. ASTM G46-94 stipulates that an average of the 10 deepest pits and the size of deepest pit (based on relative pit depth measurement after removal of corrosion products) should be used for pit damage characterization for the sample. A systematic stitching approach was adopted whereby 9 different 3 x 3 mm^2 areas were analyzed to cover a sample surface area of 9 x 9 mm^2. Consequently, 3D images of regions on the sample surface where the deepest pits exist were identified and measured.

RESULTS AND DISCUSSION

Electrochemical Characteristics and Corrosion product formation

This section focuses on the corrosion characteristics leading to the formation of corrosion products in H$_2$S-containing corrosion systems. This is based on a combination of the electrochemical response and post-experimental analysis.

<u>Effect of addition of Fe^{2+} in H$_2$S-containing environments</u>

Figure 2 presents the corrosion rate and corrosion potential measured for tests in 10% H$_2$S and 90% CO$_2$ with and without the addition of 50 ppm of Fe^{2+}. Referring to Figure 2 the corrosion rate starts at ~3.17 mm/yr for test without additional Fe^{2+} and ~3.53 mm/yr for the test with additional 50 ppm of Fe^{2+}. The corrosion rate shows a more significant reduction in corrosion rate in the environment containing 50 ppm of Fe^{2+} (final corrosion rate of ~0.4 mm/yr). This effect is lowered in the environment without additional Fe^{2+} (final corrosion rate of ~ 0.56 mm/yr). From Figure 2, it can also be observed that the key difference in the evolution of the corrosion process between the test environment with and without additional 50 ppm of Fe^{2+} is the mechanism influencing and controlling the FeS formation kinetics.
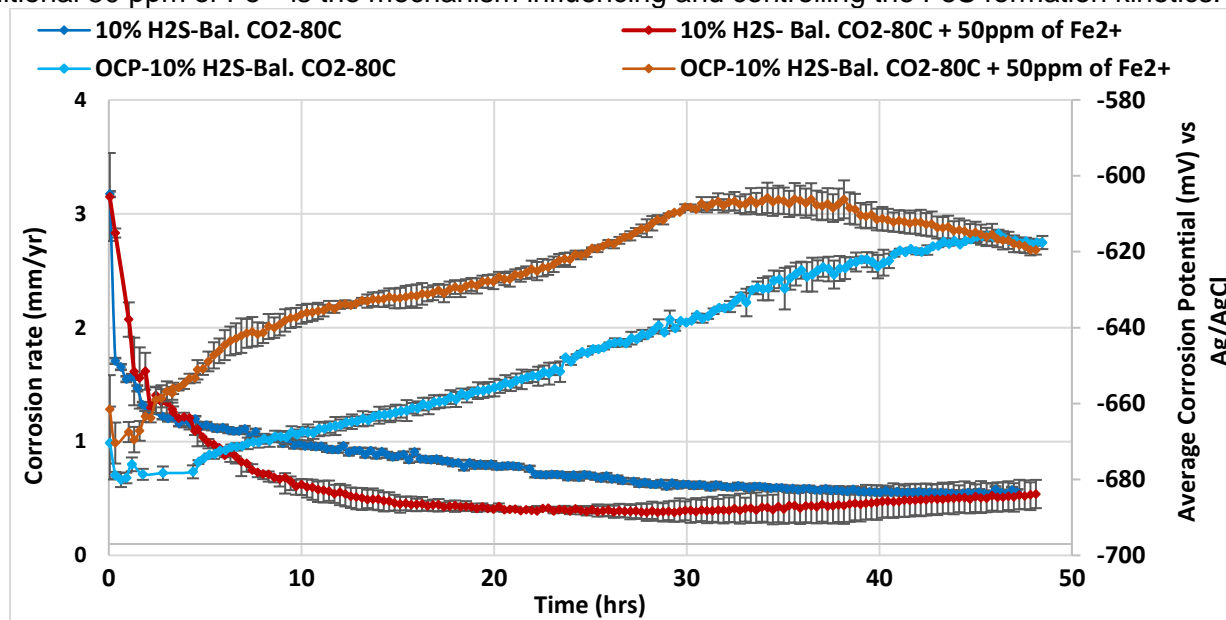
Figure 2: Corrosion rate and corrosion potential of X65 (UNS K03014) carbon steel in 1M NaCl solutions saturated with both 10% H$_2$S and 90% CO$_2$ with 0 ppm and 50 ppm of additional Fe^{2+} and without at 80°C, over 48 hours.

It is believed that the addition of 50 ppm of Fe^{2+} in the bulk might have changed the bulk chemistry and hence the corrosion interface and influence the expected mechanism of FeS formation via aqueous corrosion that often leads to the formation of crystalline FeS[4, 9] to favor the formation of an inner non-crystalline layer of FeS. The SEM images in Figure 3(a) and (b) and XRD patterns in Figure 4 show that the reduction in corrosion rate in both systems is caused by the formation of different FeS corrosion products. Although the XRD patterns presented in Figure 4 for both corrosion environments show

5

similar peaks for mackinawite with comparable intensities, the SEM images in Figure 3(a) and (b) show different morphologies of FeS formed in both systems. Although a larger quantity of FeS with highly crystalline morphology is shown in Figure 3(a) without additional 50 ppm of Fe^{2+}, the corrosion rate data show a continuous and faster rate of reduction in corrosion for test with the addition of 50 ppm of Fe^{2+}. In the latter, the FeS corrosion product formed is a mixture of three different morphologies with a more protective inner layer as shown in Figure 3(b). The corrosion potential measured over the duration of the test shown in Figure 2 also shifts towards more anodic potential values as the corrosion rate is reducing, This is an indication that the reduction of corrosion rate in both systems is due to the establishment of FeS corrosion products with protective capabilities. Figure 2 also shows that while the final corrosion potential was similar (at -617mV for the test without additional 50 ppm of Fe^{2+} and -619mV for the tests with additional 50 ppm of Fe^{2+}), the potential profiles show distinct changes with time that reflects the difference in the mechanisms behind the formation of FeS in these systems.

(a)   (b)
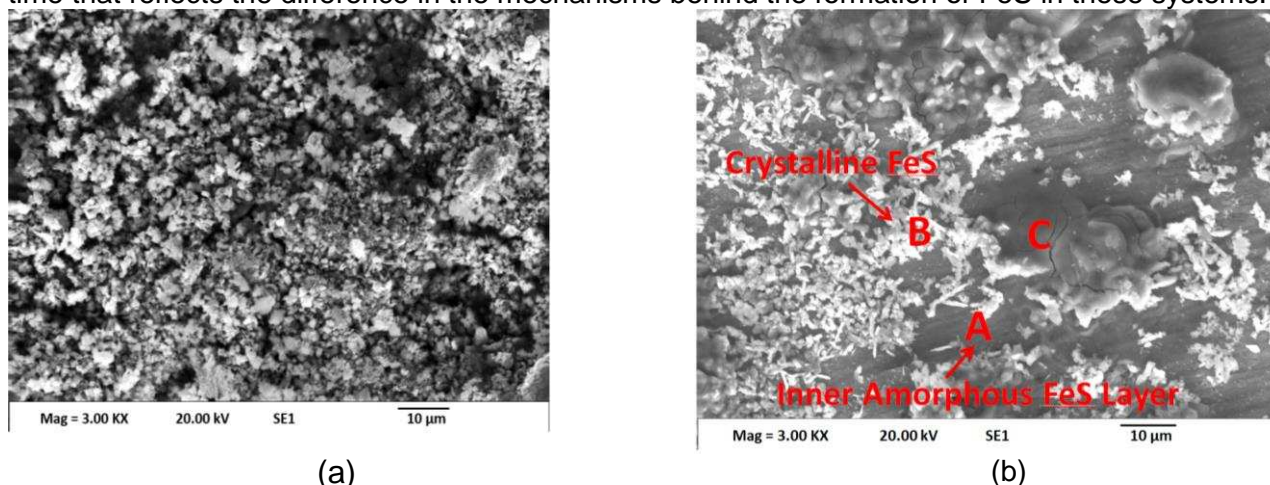
Figure 3: SEM images of corrosion product layer on X65 (UNS K03014) carbon steel in 1M NaCl solution saturated with 10% H_2S and 90% CO_2 (a) with 0 ppm of additional Fe^{2+}, (b) with 50 ppm of additional Fe^{2+} at 80℃, after 48 hours.

Referring to the SEM image presented in Figure 3(b) with 50 ppm of Fe^{2+}, the region labelled "A" is the inner nanoscale-polycrystalline FeS layer already described in previous publications [9, 10], while the region labelled "B" is an outer disperse FeS crystals. The third morphology is a distinct FeS corrosion product. This is labelled as region "C" in Figure 3(b). This clearly shows the evidence of competing mechanisms for FeS corrosion product formation. It still unclear from this study if the crystalline mackinawite in Figure 3(b) is formed from either Fe^{2+} from the CO_2 corrosion component and/or Fe^{2+} introduced into the corrosion environment. The XRD pattern in Figure 4 confirms the formation of mackinawite in this system. It is has been shown from previous studies [9] that CO_2 corrosion promotes the formation of Fe^{2+}, and indirectly contributes to the formation of large quantities of FeS similar to what has been shown in Figure 3(a) in terms of its protective properties. The deposits on top of the inner FeS layer are clearly related to a change in the chemistry of the corrosion interface as a result of additional Fe^{2+} into the corrosion system. However, the mechanism for its formation is not known and further investigation is needed to clearly understand its formation. Nonetheless, from Figure 3(b), it is believed that a combination of Fe^{2+} from the corrosion process attributed to CO_2 and the additional 50 ppm of Fe^{2+} may be enhancing the kinetics for the formation of the mixture of FeS corrosion products on the surface from three different mechanisms.
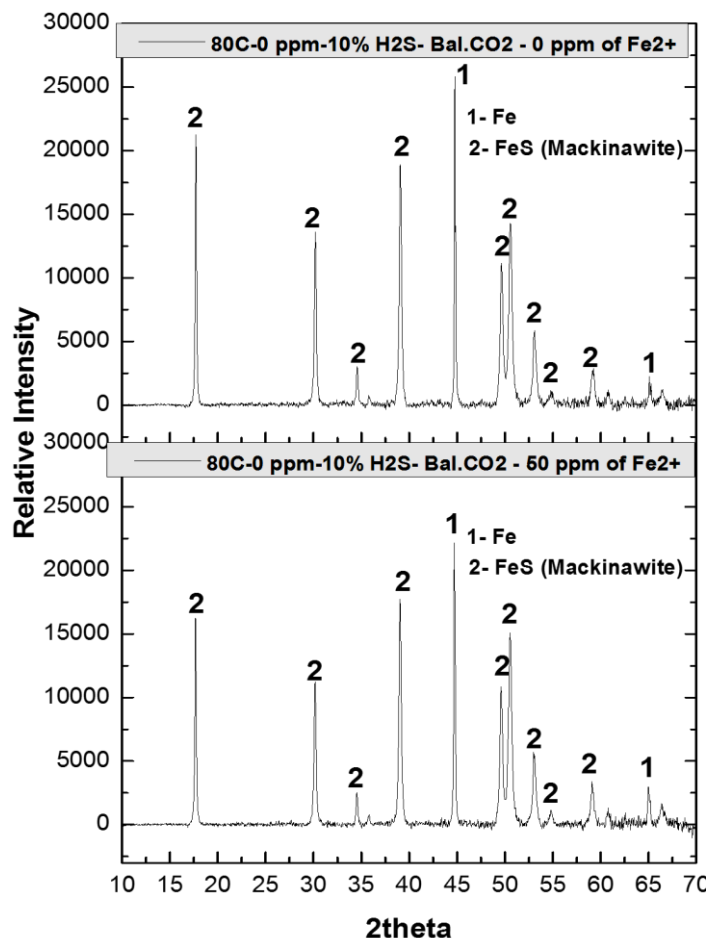
Figure 4: XRD pattern of corrosion product layer on X65 (UNS K03014) carbon steel in 1M NaCl solution saturated with 10% H₂S and 90% CO₂ with 0 ppm of additional Fe²⁺ and with 50 ppm of additional Fe²⁺ at 80°C, after 48 hours.

<u>Effect of mixture of other divalent cations (Ca²⁺ and Mg²⁺)</u>

Figure 5 presents the corrosion rate and corrosion potential data for tests in 1M NaCl as simple brine and Forties brine as a complex brine. Forties brine chemistry contains a mixture of monovalent and divalent salts (~3000 ppm of Ca^{2+} and ~1200 ppm of Mg^{2+} and other divalent cations such as Ba^{2+} and Sr^{2+}) as shown in Table 2.

Referring to Figure 5, the corrosion rate starts at ~ 3.17 mm/yr in 1M NaCl and a lower value of ~2.83 mm/yr in the complex brine. This initial difference in corrosion rate could be related to the pH of the corrosion environment. Within the first 5 hours of the tests, the rate of reduction in corrosion rate is observed to be faster for the test in the simple brine than for the test in the complex brine. This initial period of higher corrosion rate usually correlates with higher levels of dissolution of Fe^{2+}. However, between 7 and 15 hours, the corrosion rate is lower for the test in the Forties brine (~0.76 mm/yr in the Forties brine and ~0.9 mm/yr in the simple brine). Between 20 and 48 hours the corrosion rate is observed to be slightly higher in the Forties brine than in the simple brine. The observed corrosion behavior captured in the measured corrosion rate is an indication of a more dynamic and constantly changing mechanism of FeS formation in Forties brine. As mentioned earlier, the ennoblement of the OCP from the starting potential is an indication of the protective capabilities of FeS. However, from Figure 5, the final potential in the simple brine environment (at ~-617mV) is more anodic than the final potential in Forties brine (at ~621mV). This correlates well with the final corrosion rate that shows a slightly higher value (~0.69 mm/yr) in the Forties brine than in the simple brine (~0.55mm/yr). While it is important to acknowledge that this difference is small, it is equally important to state that the reduction in corrosion rate in both brines is caused by the formation of FeS as shown by the SEM images in Figure 6(a)-(c) and the XRD pattern in Figure 7. However, the difference in the profile of the corrosion

potential and corrosion rate indicates the formation of FeS by different mechanisms in both corrosion systems. Such difference in mechanisms could be due to either the effect of complex ions contained in Forties brine on the corrosion environment in form of interfacial pH or the effect of the presence of cations contained in Forties brine on the properties of FeS formed. However, the consequences of these differences in mechanism are reflected in the corrosion rate, corrosion potential profile and the formation of a more crystalline FeS in the simple brine and an amorphous form of FeS in the complex brine as shown in Figure 6(a), (b) and (c).
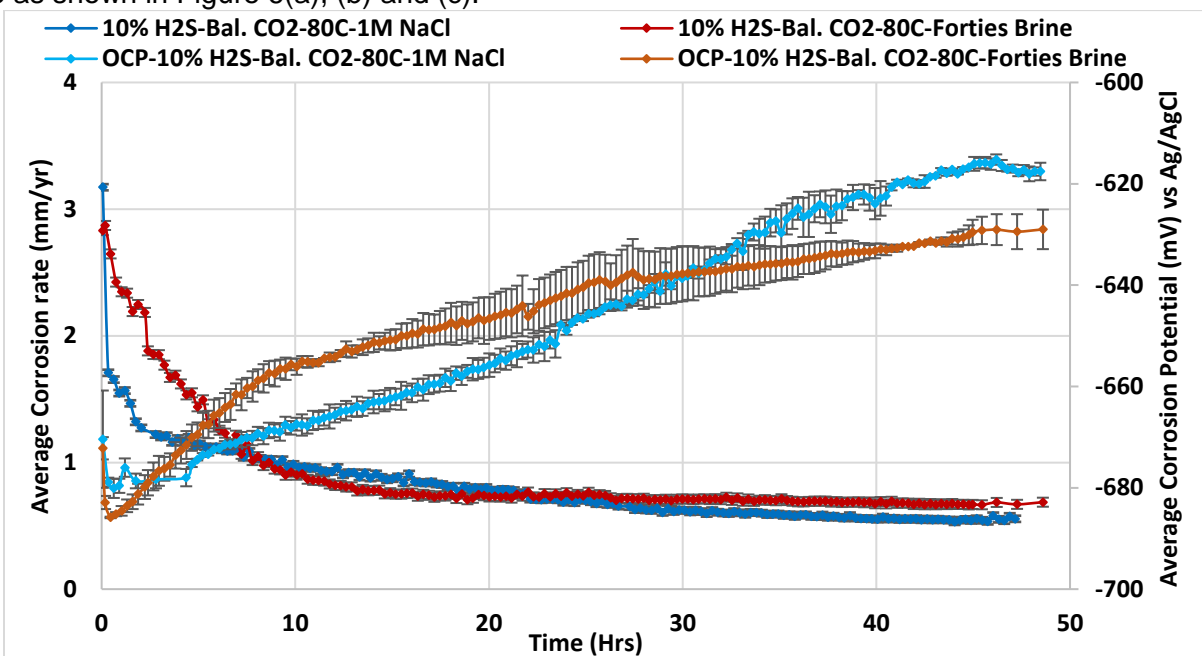
Figure 5: Corrosion rate of X65 (UNS K03014) carbon steel in 1M NaCl and Forties brine (~3000 ppm of Ca^{2+},~1200 ppm of Mg^{2+}, ~52 ppm Ba^{2+} and ~150 ppm Sr^{2+}) solutions saturated with both 10% H_2S and 90% CO_2 at 80℃, over 48 hours.

Based on earlier discussion in this paper and previous studies [9] on the effect of CO_2 in H_2S-corrosion environment, it was expected that the extended periods of higher corrosion rate would lead to an increase in availability of Fe^{2+} for the formation of FeS. Figure 6(a) confirms this and also it is clear that FeS has a largely crystalline but porous morphology. Figure 6(b) shows a FeS rich layer that is dense and appears amorphous. Local areas where the film has ruptured are clear. From Figure 6(c), there is a clear build-up of stresses within this film. The presence of Ca^{2+}/Mg^{2+} and other divalent cations (present in Forties brine) in the corrosion interface may have poisoned the formation of crystalline FeS formed in 1M NaCl and limited the formation of FeS to an amorphous corrosion layer. This effect could also be related to the pH of the corrosion environment which could be as a result of buffering effect from the complex ions contained in Forties brine. Forties brine is known to have a slightly higher pH than simple NaCl brine. The pH influence on the thermodynamics of FeS films has been linked to the stability of mackinawite film across an increasing range of H_2S partial pressure [15, 16]. Smith et al [16] suggested that a neutral pH of 7 increases the stability of mackinawite to higher H_2S levels at low and moderate temperatures, while a more acidic pH (for example pH of 4) would potentially increase the tendency for the formation of pyrrhotite and/or transition from mackinawite to pyrrhotite at low H_2S levels, thereby reducing the size of the mackinawite stability range. The latter has been shown in previous publications [9]. This current work suggests that in addition to changing the transition and stability of one thermodynamic state whether it is crystalline or amorphous may also be influenced by changing solution pH. This may also be contributing to loss of integrity and final breakdown of iron sulphide corrosion product layers [16-18].

It is believed that corrosion film rupture shown in Figure 6(b) and (c) could be related to the internal epitaxial stresses built-up as a result of formation of mackinawite with larger volumes than the volume of Fe^{2+} consumed for its formation. This is often defined as the Pilling-Bedworth (P-B) ratio [19]. This

ratio measures the fraction of corroded iron that is captured in the corrosion layer and defined as the ratio of the volume of the metal corrosion product to the consumed metal volume. While this ratio has been defined for passive oxide layers, it is important to note that this mechanism of film rupture can also occur in non-passivating metallic alloys such as carbon steel in oilfield environments. As clearly observed in Figure 6(b) and (c), there is precipitation of crystalline FeS underneath the nano-scale polycrystalline FeS, which may have caused the epitaxial stresses and film rupture or have been formed after film rupture. The true chemistry has not yet been confirmed in this study but XRD analysis showed a weak peak for mackinawite at ~18˚ 2theta[20] and a predominantly non-crystalline layer.

(a)

(b)

(c)
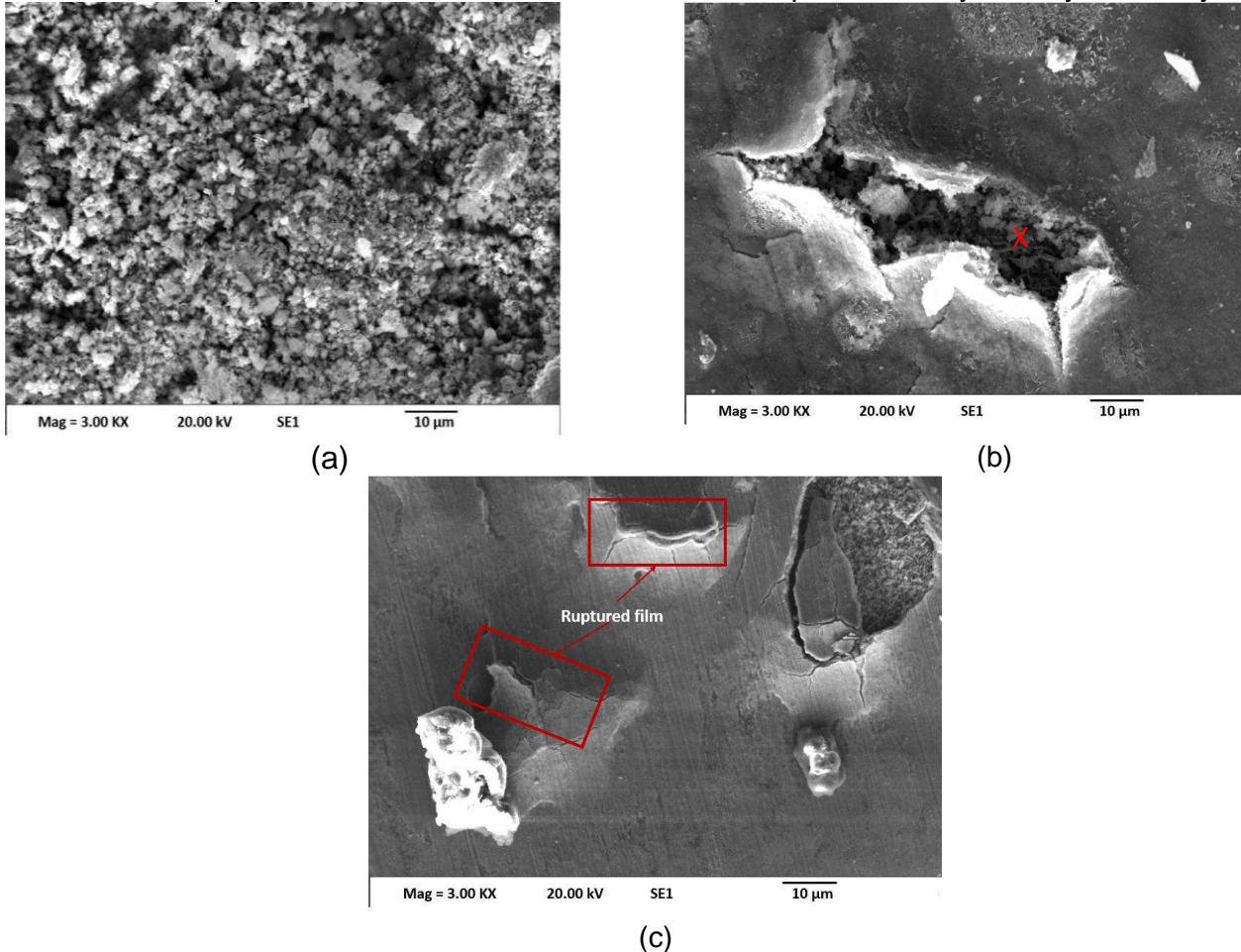
Figure 6: SEM images of corrosion product layer on X65 (UNS K03014) carbon steel (a) in 1M NaCl, (b) Forties brine (~3000 ppm of Ca^{2+}, ~1200 ppm of Mg^{2+}, ~52 ppm Ba^{2+} and ~150 ppm Sr^{2+}) and (c) Forties brine (~3000 ppm of Ca^{2+}, ~1200 ppm of Mg^{2+}, ~52 ppm Ba^{2+} and ~150 ppm Sr^{2+}) (showing a different region of the test sample) solutions saturated with 10% H_2S and 90% CO_2 at 80°C, after 48 hours.
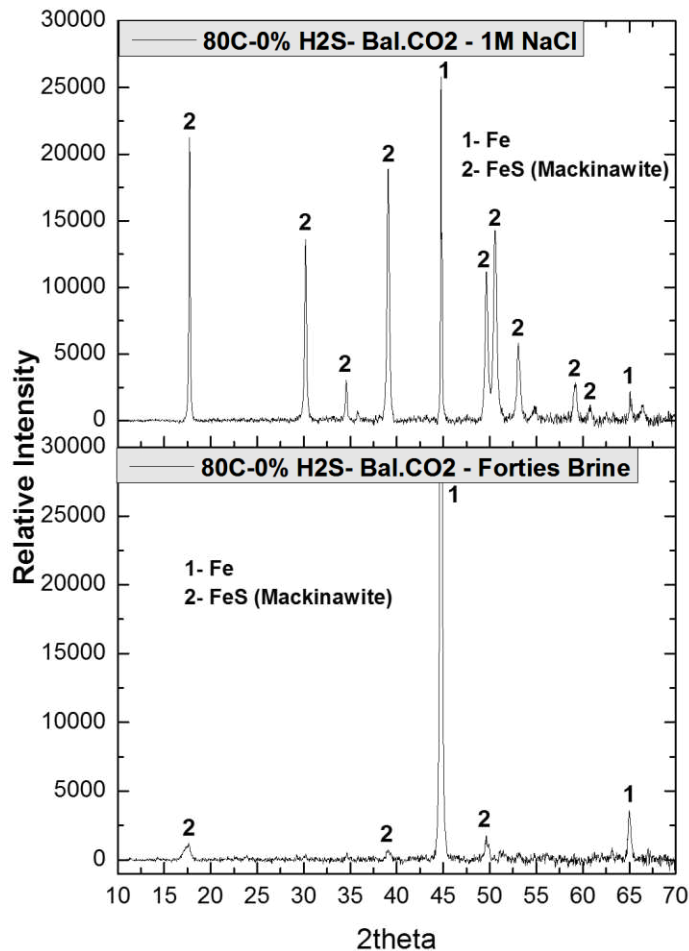
Figure 7: XRD pattern of corrosion product layer on X65 (UNS K03014) carbon steel in 1M NaCl and Forties brine (~3000 ppm of Ca^{2+},~1200 ppm of Mg^{2+}, ~52 ppm Ba^{2+} and ~150 ppm Sr^{2+}) solutions saturated with both 10% H_2S and 90% CO_2 at 80°C, over 48 hours.

Pitting corrosion characteristics after 48 hrs

This section discusses the process of initiation of pitting corrosion. Referring to corrosion potential data in Figure 2 and Figure 5, it is evident that the process of formation of FeS corrosion product induces significant changes in the corrosion interface to protect the corroding surface and causing a change in corrosion potential of between ~50 – 70 mV. It has also been shown in a previous publication[9] and supported by other authors[21] that such changes in corrosion potential between bare steel and steel with corrosion products are capable of inducing significant galvanic effect to support pit initiation and growth. Another important property of FeS is its ability to support electrochemical reactions across the corrosion interface[22]. As shown in Figure 2 and Figure 5, the extent and profile of changes in corrosion potential are seen as an intrinsic characteristic of the corrosion system.

Effect of addition of Fe^{2+} in H_2S-containing environments on pitting corrosion process

As already discussed in earlier sections of this paper, addition of 50 ppm of Fe^{2+} to 10% H_2S-containing corrosion environment has been shown to alter the morphology of the FeS film. In addition to an inner amorphous FeS layer there is also the formation of crystalline FeS and a third morphology in the corrosion product. Figure 8 and 9 present data from it pitting corrosion characterization and it clearly shows that the addition of Fe^{2+} accelerates the average and deepest pit depths in addition to increasing the number of pits. This is opposite to the effect it has on general corrosion.
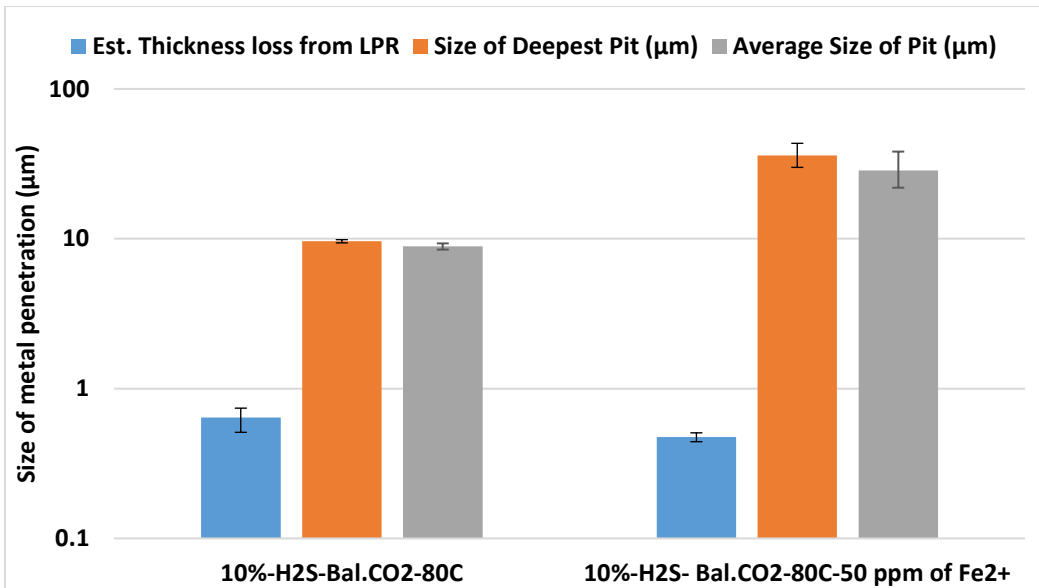
Figure 8: Graph showing estimated thickness loss from general corrosion measurements, the size of deepest pit and the average of the 10 deepest pits on 81% of the exposed surface of X65 (UNS K03014) carbon steel in 1M NaCl solutions saturated with both 10% H_2S and 90% CO_2 with and without the addition of 50 ppm of Fe^{2+} at 80°C, over 48 hours. Note that error bars represent an average of 2-3 separate measurements from 2-3 repeatable experiments for each of the data shown.
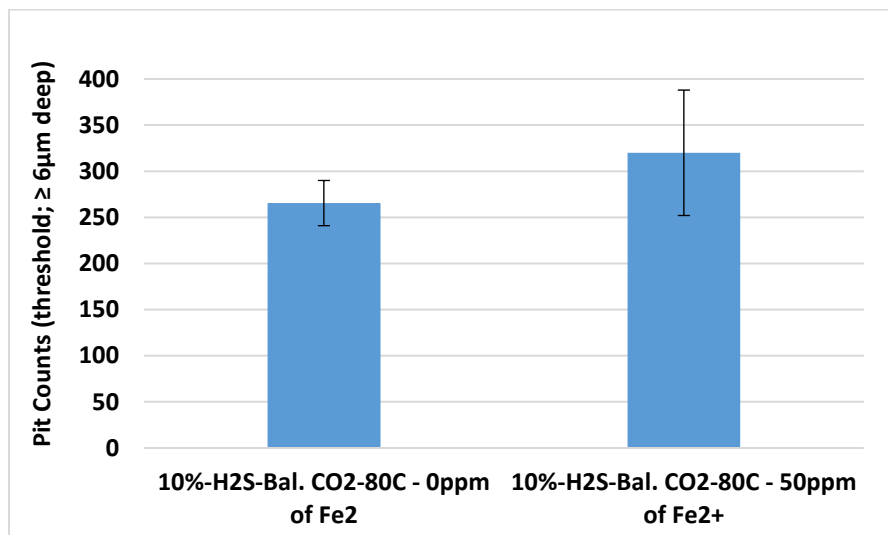
Figure 9: Graph showing the number of pits ≥ 6 µm in depth on 81% of the exposed surface of X65 (UNS K03014) carbon steel in 1M NaCl solutions saturated with 10% H_2S and 90% CO_2 with and without the addition of 50 ppm of Fe^{2+} at 80°C, over 48 hours.

The pit morphology shown in Figure 10(a) an (b) is also shown to be affected by the addition of 50 ppm of Fe^{2+}. From the images in Figure 10(a) and (b), there is evidence of protection of areas of the steel surface surrounding the pits in tests with additional Fe^{2+}, which is not the case without additional Fe^{2+}. This shows that while the corrosion rate profile shown in Figure 2 appears similar for most part of the corrosion process for both corrosion systems, a significant percentage of the corroding surface is being protected by the complex mixture of FeS formed in the test with additional 50 ppm of Fe^{2+} leading to severe pitting corrosion on areas not fully protected as shown in Figure 8 and 10(b). The electronic property of FeS is perhaps relevant in this case to drive pitting corrosion process[9,10]. The diameter of the pits in this case is also larger with 50 ppm of Fe^{2+} than with 0 ppm of Fe^{2+}.

(a)   **(b)**
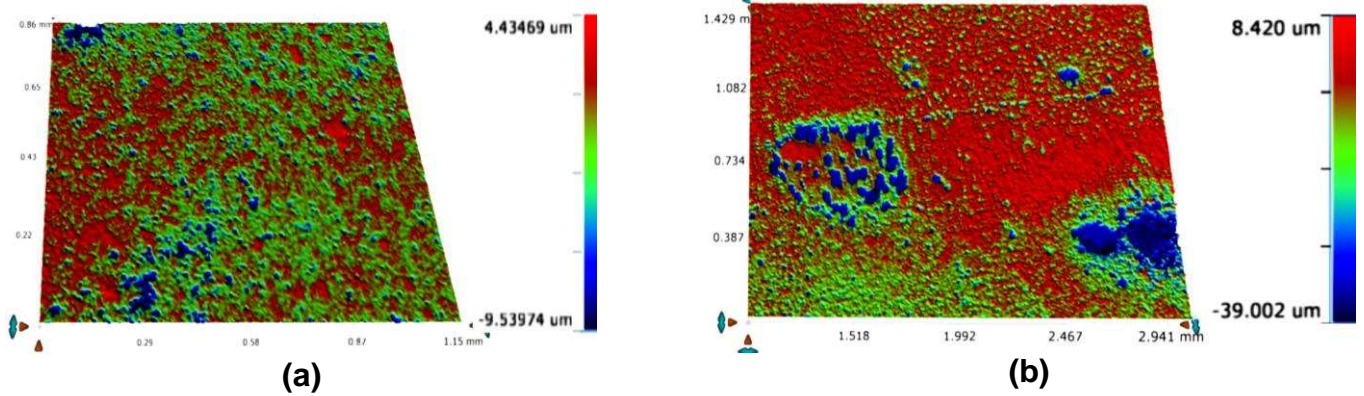
Figure 10: 3D image of the deepest pit on 81% of the exposed surface of X65 (UNS K03014) carbon steel in 1M NaCl solutions saturated with (a)10% H_2S and 90% CO_2 with 0 ppm of Fe^{2+} and (b) 10% H_2S and 90% CO_2 with 50 ppm of Fe^{2+} at 80℃, over 48 hours.

Effect of mixture of other divalent cations (Ca^{2+} and Mg^{2+}) on pitting corrosion process

As already discussed and shown in Figure 5 and 6, the introduction of ~3000 ppm of Ca^{2+},~1200 ppm of Mg^{2+}, ~52 ppm Ba^{2+} and ~150 ppm Sr^{2+} ions has been shown to influence the formation of FeS. It is believed that the restriction of FeS corrosion morphology to an amorphous layer even with similar amount of Fe^{2+} to the test in simple brine may have caused the build-up of a thick layer of FeS. As shown in Figure 6(b) and (c), this layer of FeS has been observed to have ruptured due to an internal epitaxial stress within the corrosion product layer. This is evident from the formation of crystalline FeS within the ruptured region leading to the initiation of larger size pits; an average of ~35 µm compared to pit size of ~10µm in 1M NaCl solution. The amount of ferrite made available in both systems is similar as shown by the estimated thickness loss to general corrosion in Figure 11. The observation of evolution of pitting corrosion is consistent with other authors that have suggested that internal epitaxial stresses often leads to micro-cracking and eventually delamination (see Figure 6(b) and (c)) and breakdown of the mackinawite film [17, 23, 24], which are the most likely precursors for localised and pitting corrosion.
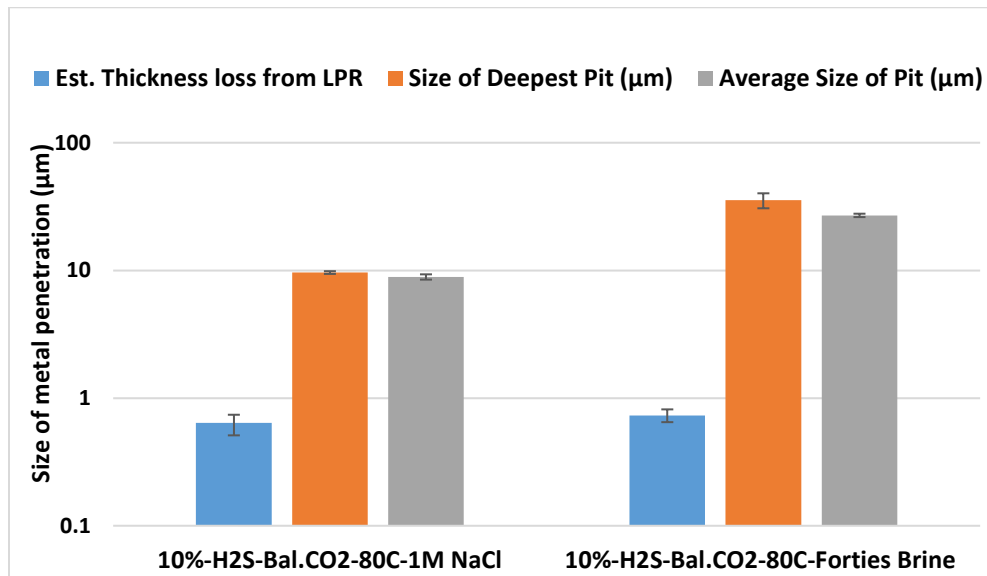
Figure 11: Graph showing the thickness loss to general corrosion, the size of deepest pit and the average of the 10 deepest pits on 81% of the exposed surface of X65 (UNS K03014) carbon steel in 1M NaCl and Forties brine (~3000 ppm of Ca^{2+},~1200 ppm of Mg^{2+}, ~52 ppm Ba^{2+} and ~150 ppm Sr^{2+}) solutions saturated with both 10% H_2S and 90% CO_2 at 80℃, over 48 hours. Note that both experiments were repeated three times and the error bars on pit data represents the average of two repeatable data.

Figure 12 shows that the average number of pits per 1 cm^2 of sample size is the same for both brines (as was the estimated thickness loss due to uniform corrosion) but the morphology of pitting corrosion attack is different with tests in complex brine. Severe pitting attack is demonstrated by the larger size of the measured pits than in simple brine. These observations are also consistent with is the level of protection surrounding the well defined open-mouthed pits. It is believed that the Fe^{2+} generated and captured in the general corrosion rate may be generated within the local pits/areas of film rupture. This is because the surface surrounding the pits appears to be protected by the amorphous layer as against the surface underneath a large deposit of crystalline FeS (See Figure 6(a), (b) and (c). This is a strong indication that pit initiation by FeS based corrosion product in Forties brine is due to the rupture of corrosion film from internal stresses within the film.
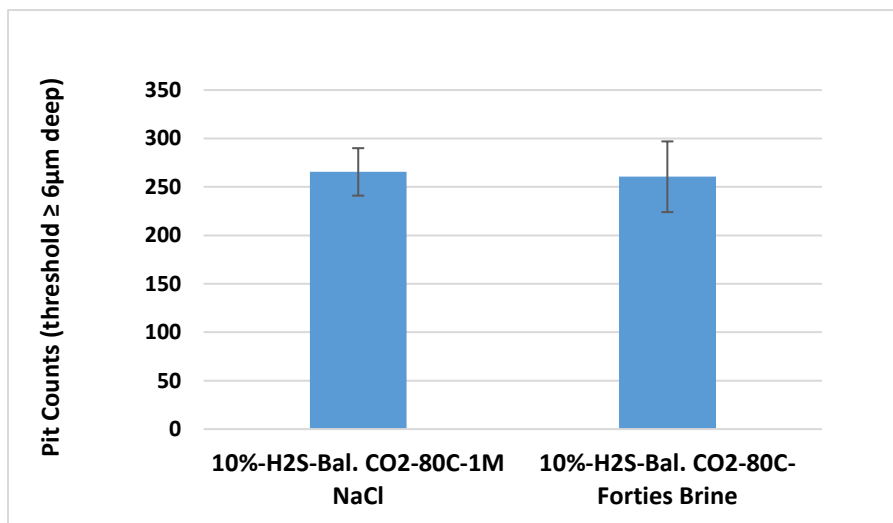
Figure 12: Graph showing the number of pits ≥ 6 μm in depth on 81% of the exposed surface of X65 (UNS K03014) carbon steel in 1M NaCl and Forties brine (~3000 ppm of Ca^{2+},~1200 ppm of Mg^{2+}, ~52 ppm Ba^{2+} and ~150 ppm Sr^{2+}) solutions saturated with both 10% H_2S and 90% CO_2 at 80℃, over 48 hours. Note that both experiments were repeated three times and the error bars on pit data represents the average of two repeatable data.

(a)   (b)
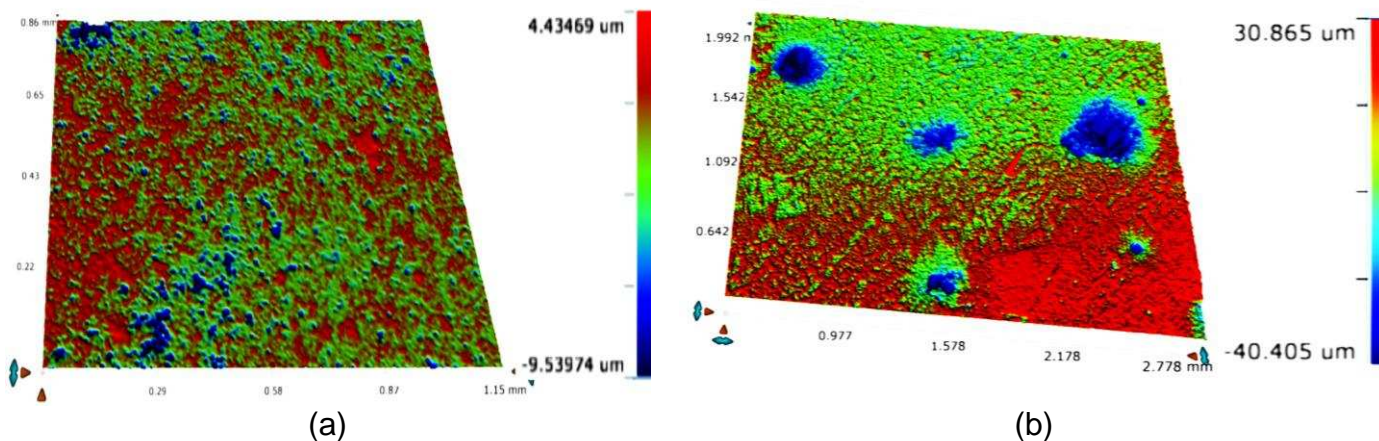
Figure 13: 3D image of the deepest pit on 81% of the exposed surface of X65 (UNS K03014) carbon steel in (a)1M NaCl and (b) Forties brine (~3000 ppm of Ca^{2+},~1200 ppm of Mg^{2+}, ~52 ppm Ba^{2+} and ~150 ppm Sr^{2+})solutions saturated with 10% H_2S and 90% CO_2 at 80℃, over 48 hours.

CONCLUSIONS

The general and localized corrosion characteristics of carbon steel in H_2S-containing corrosion system have been investigated in the presence of multiple divalent cations. The following conclusions are presented.

1. The overall corrosion characteristics of carbon steel in a H$_2$S-contaning system at 80°C are influenced significantly by the competing mechanisms for FeS formation; direct reduction and precipitation. The source and concentration of Fe^{2+} in the corrosion interface is an important factor in determining which of the competing mechanisms becomes dominant. It also affects the form of FeS film that is formed.

2. The presence of an additional 50 ppm of Fe^{2+} in the bulk electrolyte modifies the corrosion interface to promote the formation of a combination of three different morphologies of FeS (Mackinawite); amorphous FeS, crystalline FeS and a third non-crystalline FeS corrosion product. The changes associated with the addition of Fe^{2+} also increase the severity of pitting corrosion. The morphology of pitting attack is significantly affected. This is potentially due to the formation of an oxide-rich corrosion product.

3. The presence of other divalent cations from the use of Forties brine (~3000 ppm of Ca^{2+}, ~1200 ppm of Mg^{2+}, ~52 ppm Ba^{2+} and ~150 ppm Sr^{2+}) appears to restrict the morphology of FeS to an amorphous outer layer and crystalline inner layer. This is also observed to increase the severity of pitting corrosion damage. The morphology of initiated pits is also significantly affected. This is possibly due the type of film formed and the mode of its rupture.

REFERENCES

1. M.B. Kermani and D. Harrop, "The impact of corrosion on oil and gas industry", SPE Production & Operations, 11, 3 (1996): p. 186-190.
2. B.M. Kermani and A. Morshed, "Carbon dioxide corrosion in oil and gas production: A compendium", Corrosion, 59, 08 (2003): p. 659-683.
3. E. Abelev, J. Sellberg, T.A. Ramanarayanan, and S.L. Bernasek, "Effect of H$_2$S on Fe corrosion in CO$_2$-saturated brine", Journal of Materials Science, 44, 22 (2009): p. 6167-6181.
4. S.N. Smith. "Current understanding of corrosion mechanisms due to H2S in oil and gas production environments", CORROSION, Paper no. 5485, (Dallas, TX: NACE International 2015, 2015).
5. M. Singer, B. Brown, A. Camacho, and S. Nešić, "Combined effect of carbon dioxide, hydrogen sulfide, and acetic acid on bottom-of-the-line corrosion", Corrosion, 67, 1 (2011): p. 015004-1-015004-16.
6. Y. Zheng, B. Brown, and S. Nešić, "Electrochemical study and modelling of H2S corrosion of mild steel", Corrosion, 70, 4 (2013): p. 351-365.
7. D.W. Shoesmith, P. Taylor, M.G. Bailey, and D.G. Owen, "The Formation of Ferrous Monosulfide Polymorphs during the Corrosion of Iron by Aqueous Hydrogen Sulfide at 21°C", Journal of The Electrochemical Society, 127, 5 (1980): p. 1007-1015.
8. Y. Zheng, J. Ning, B. Brown, and S. Nešić, "Electrochemical Model of Mild Steel Corrosion in a Mixed H$_2$S/CO$_2$ Aqueous Environment in the Absence of Protective Corrosion Product Layers", Corrosion, 71, 3 (2015): p. 316-325.
9. F. Pessu, R. Barker, and A. Neville, "Pitting and Uniform Corrosion of X65 Carbon Steel in Sour Corrosion Environments: The Influence of CO2, H2S, and Temperature", CORROSION, 73, 9 (2017): p. 1168-1183.
10. F. Pessu, Y. Hua, R. Barker, and A. Neville, "A Study of the Pitting and Uniform Corrosion Characteristics of X65 Carbon Steel in Different H$_2$S-CO$_2$-Containing Environments", CORROSION, 74, 8 (2018): p. 886-902.
11. H. Ma, X. Cheng, G. Li, S. Chen, Z. Quan, S. Zhao, and L. Niu, "The influence of hydrogen sulfide on corrosion of iron under different conditions", Corrosion Science, 42, 10 (2000): p. 1669-1683.
12. Y. Hua, A. Shamsa, R. Barker, and A. Neville, "Protectiveness, morphology and composition of corrosion products formed on carbon steel in the presence of Cl$^-$, Ca^{2+} and Mg^{2+} in high pressure CO$_2$ environments", Applied Surface Science, 455, (2018): p. 667-682.

13. X. Jiang, Y.G. Zheng, D.R. Qu, and W. Ke, "Effect of calcium ions on pitting corrosion and inhibition performance in CO_2 corrosion of N80 steel", Corrosion Science, 48, 10 (2006): p. 3091-3108.
14. ASTM Standard G46-94, Standard guide for examination and evaluation of pitting corrosion. ASTM International: West Conshohocken, PA, 2003.
15. R. Woollam, K. Tummala, J. Vera, and S. Hernandez. "Thermodynamic prediction of $FeCO_3$-FeS corrosion product films", CORROSION, paper no. 076, (Houston, TX.: NACE International, Houston, Texas, 2011).
16. S.N. Smith, B. Brown, and W. Sun. "Corrosion at higher H_2S concentrations and moderate temperatures", CORROSION, paper no. 81, (Houston, TX.: NACE International, Houston, Texas, 2011).
17. S. Nesic, H. Li, J. Huang, and D. Sormaz. "An open source mechanistic model for CO_2 / H_2S corrosion of carbon steel", CORROSION, paper no. 572, (Atlanta, GA.: NACE International, Houston, Texas, 2009).
18. B. Brown and S. Nesic. "Aspects of localized corrosion in an H_2S-CO_2 environment", CORROSION, paper no. 1559, (Salt Lake City, UT.: NACE International, Houston, Texas, 2012).
19. M. Schütze, R.W. Cahn, and E.J. Kramer, Corrosion and Environmental Degradation: A Comprehensive Treatment. 2000: Wiley-VCH.
20. A. R. Lennie, S. A. T. Redfern, P. F. Schofield, and D.J. Vaughan, "Synthesis and rietveld crystal structure refinement of mackinawite, tetragonal FeS", Mineralogical Magazine, 59, (1995): p. 6.
21. J. Han, B.N. Brown, and S. Nešić, "Investigation of the galvanic mechanism for localized carbon dioxide corrosion propagation using the artificial pit technique", Corrosion, 66, 9 (2010): p. 12.
22. H.-H. Huang, W.-T. Tsai, and J.-T. Lee, "Corrosion morphology of A516 carbon steel in H_2S solution", Scripta Metallurgica et Materialia, 31, 7 (1994): p. 825-828.
23. J. Kvarekval. "Corrosion Layer breakdown and Localized Corrosion in H_2S-CO_2 Environments", NACE International, (Houston, Texas, 2012).
24. S. Nesic, S. Wang, H. Fang, W. Sun, and J.K.-L. Lee. "A new updated model of CO_2-H_2S corrosion in multiphase flow", CORROSION, paper no. 535, (New Orleans, LA: NACE International, 2008).